Object-Based Image Analysis and Digital Terrain Analysis for Locating Landslides in the Urmia Lake Basin, Iran

Thomas Blaschke, Bakhtiar Feizizadeh, and Daniel Hölbling

***Abstract*—The main objective of this research was to establish a semiautomated object-based image analysis (OBIA) methodology for locating landslides. We have detected and delineated landslides within a study area in north-western Iran using normalized difference vegetation index (NDVI), brightness, and textural features derived from satellite imagery (IRS-ID and SPOT-5) in combination with slope and flow direction derivatives from a digital elevation model (DEM) and topographically oriented gray-level cooccurrence matrices (GLCMs). We utilized particular combinations of these information layers to generate objects by applying multiresolution segmentation in a sequence of feature selection and object classification steps. The results were validated by using a landslide inventory database including 109 landslide events. In this study, a combination of these parameters led to a high accuracy of landslide delineation yielding an overall accuracy of 93.07%. Our results confirm the potential of OBIA for accurate delineation of landslides from satellite imagery and, in particular, the ability of OBIA to incorporate heterogeneous parameters such as DEM derivatives and surface texture measures directly in a classification process. The study contributes to the establishment of geographic object-based image analysis (GEOBIA) as a paradigm in remote sensing and geographic information science.**

***Index Terms*—GIScience, gray-level cooccurrence matrix (GLCM), landslide mapping, object-based image analysis (OBIA), remote sensing, rule-based classification, textural analysis.**

I. Introduction

THE RECOGNITION and delineation of landslides is a critical task for pre- and postdisaster analysis [1]–[3]. Geoinformation, in particular, satellite imagery, plays a key role in the detection, analysis, and monitoring of landslides for hazard and risk analysis [4]. In general, remote sensing techniques such as aerial photography interpretation, stereoscopic image analysis, and interferometry studies can be used to detect, monitor, and classify landslides [5]. A wide range of global observation data available enable rapid and accurate investigations of landslides to be made, facilitating the generation of landslide inventory maps and databases [4]. Nevertheless, the authors have observed that the majority of applications still use a "per-pixel" approach to remote sensing data [6], relying mainly on the reflectance values of the different spectral bands and multivariate statistics.

Object-based image analysis (OBIA) has gained prominence in the field of remote sensing over the last decade. It is credited to have the potential to overcome weaknesses associated with per-pixel analysis such as, for instance, disregarding geometric and contextual information [6], [7]. When it is used within the "geo-domain" or at scales which are related to earth (geo)-centric applications, it is in scientific literature often referred to as geographic object-based image analysis (GEOBIA) (see Blaschke [6] for a comprehensive discussion). OBIA is a knowledge-driven approach in which a range of diagnostic features for a particular object can be integrated on the basis of expert knowledge [5], [8], [9]. This approach aims to represent the content of a complex scene in a manner that best describes the imaged reality, by mimicking human perception [10]. By incorporating spectral information (e.g., color) and spatial characteristics (e.g., size, shape), together with textural data and contextual information (e.g., association with neighboring objects), OBIA approaches the way that humans visually interpret the information on aerial photos and satellite images [5], [10], [11]. This ability has been demonstrated by dozens of applications [6].

In this context, landslide detection and delineation through earth observation data are considered to be a promising application domain. Despite the ability of OBIA to integrate remote sensing imagery with GIS datasets, object-based approaches to landslide mapping remain relatively rare. To this end, the potential of OBIA for (semi-) automated landslide detection has consequently yet to be fully explored or exploited [2], and only relatively few studies applied OBIA to digital elevation models (DEMs) and their derivatives [2], [13], [14]. Particularly, while building on the work of Martha *et al.* [2] and Hölbling *et al.* [4], we hypothesize that OBIA has a high potential for landslide investigations, as it is able to reflect spectral, spatial, contextual, and morphological parameters in an integrative manner [4]. In this paper, we want to take this one step further and to prove

Manuscript received November 16, 2013; revised March 31, 2014; accepted June 01, 2014. Date of publication September 18, 2014; date of current version January 21, 2015. This work was supported in part by the Austrian Science Fund FWF through the Doctoral College GIScience under Grant DK W 1237-N23 and in part by the stand-alone project iSLIDE under Grant P 25446-N29 through the University of Salzburg.

T. Blaschke is with the Interfaculty Department of Geoinformatics—Z_GIS, University of Salzburg, 5020 Salzburg, Austria, and also with the Research Studio Austria FG, Studio iSPACE, 5020 Salzburg, Austria (e-mail: thomas.blaschke@sbg.ac.at).

B. Feizizadeh is with the Centre for Remote Sensing and GIS, Department of Physical Geography, University of Tabriz, Tabriz 51368, Iran (e-mail: Feizizadeh@tabrizu.ac.ir).

D. Hölbling is with the Interfaculty Department of Geoinformatics—Z_GIS, University of Salzburg, 5020 Salzburg, Austria (e-mail: daniel.hoelbling@sbg.ac.at).

Color versions of one or more of the figures in this paper are available online at http://ieeexplore.ieee.org.

Digital Object Identifier 10.1109/JSTARS.2014.2350036

through our research the ability of OBIA to act as a lynchpin for the integration of spectral data with spatial data (such as elevation and thematic data). This includes the combined use of textural information, shape, size, and neighboring features whereby all these factors are considered to be relevant for landslide detection [5]. Since landslides can occur within diverse and complex geomorphologic settings, it is essential to consider landslides within the context of their surroundings. We have therefore used this principle to develop a semiautomated OBIA workflow, which we then applied to a study area in northwestern Iran.

II. Methods

A. Study Area and Data

The study area formed part of the Urmia Lake basin in northwestern Iran. Landslides are common within this basin [15] due to unstable slopes in complicated tectonic settings [16], [17]. A landslide inventory database for this area was available from the Ministry of Natural Resources, East Azerbaijan Province, Iran. This database includes records of the occurrence of 109 landslide events whose GPS coordinates were recorded during field surveys [18]. A single representative point was stored for each landslide, but no outlines were recorded for the areas affected by individual events. Accordingly, one objective of this study was therefore to derive the spatial coverage of the individual landslides. For this delineation exercise, we used a multispectral SPOT-5 satellite image from May 05, 2005 with 10-m spatial resolution, and an IRS-ID P6 panchromatic satellite image from May 21, 2005, which had 5.8-m spatial resolution. A DEM derived from a 1:25 000 scale topographic map with 10-m spatial resolution was used to extract morphometric features characteristic of landslides, e.g., slope and flow direction. The widely used eCognition software environment [6], [19] was used for the OBIA [6], [20] part. Rule sets were developed using what is known as the Cognition Network Language (CNL) or is sometimes referred to as a "developer framework."

B. Image Segmentation and the OBIA Approach

Segmentation is an important stage in OBIA. It can be defined as a "partitioning process of an image into homogeneous and nonoverlapping regions that are later identified as objects" [21, p. 7103]. The choice of segmentation parameters affects the size of the image objects [5]. A multiresolution segmentation algorithm [22] is frequently used in earth science studies [6], [23]; it minimizes the average heterogeneity of image objects by applying a mutual best-fitting approach [7], [22]. Multiresolution segmentation is a bottom-up region-merging technique that merges the most similar adjacent regions (starting from individual pixels) as long as the internal heterogeneity of the resulting object does not exceed the user-defined threshold of the scale factor [19]. The eCognition software performs multiresolution segmentation on the basis of scale, color, and shape, with the shape including both compactness and smoothness [24]. Considering the complex characteristics of landslides, such as variations in land cover, differences in illumination, diversity of spectral behavior, and size variability, it is difficult to delineate each individual landslide as a single object [2], [12]. Over- and undersegmentation can, however, be reduced by using a multiscale optimization approach [10], [12]. Fig. 1 illustrates the overall workflow which is divided into three major phases.

The multiresolution segmentation approach in the eCognition software was employed for the initial segmentation. Then, the data were parameterized according to the specific requirements for mapping landslides and incorporated into a multiscale optimization routine [12]. In this way, we aimed to integrate the spectral, spatial, and morphometric characteristics of landslides. The brightness and normalized difference vegetation index (NDVI) were calculated from SPOT and IRS images, while slope and flow directions were derived from the DEM. These process domains were then segmented yielding several segmentation levels with consecutively smaller increments. The segmentation process can sometimes lead to the generation of objects that are either too small (over-segmentation) or too large (under-segmentation) and does not fully represent the objects of interest, especially when dealing with complex natural features such as landslides. Choosing an appropriate scale parameter is therefore critical in OBIA [25], [26]. We selected a relatively small-scale factor in order to be able to detect small landslides, even though this then results in a large number of objects. Subsequent merging of small objects belonging to an individual landslide complex seemed to be more straightforward than performing resegmentations on objects that were considered to be too large. The segmentation was performed using five scale parameters (5, 7, 8, 9, and 10), with the same shape (0.3) and compactness (0.5) factors. For a comprehensive discussion of scale parameters, we refer the reader to [6], [10], [26], and [27]. In general, a larger scale parameter results in larger image objects [5], [19]. The results from the previous segmentation cycle then became the subobject level for the subsequent cycle. At the next larger scale factor, a number of objects were merged to create a super-object level, as suggested by Lu *et al.* [12]. In subsequent steps, the smaller image objects were merged into larger objects on the basis of the chosen scale, color, and shape parameters, which define the growth in heterogeneity between adjacent image objects. The objects from segmentation using a scale parameter of 10 were ultimately used for further analysis.

C. Identifying Potential Landslide-Affected Areas

Following the various optimization steps, the resulting image segments were analyzed with respect to their spatial, spectral, and textural parameters. They were then classified into either "potential landslide" or "no landslide" on the basis of expert knowledge. Most of the known landslides within the study area are rotational landslides [16], [17]. The morphological characteristics of these rotational slides exhibit abrupt changes in slope morphology, with concavity in the depletion zone of the landslide and convexity in the accumulation zone [5], [27], [28].

An analysis of the landslide inventory map revealed that all of the 109 landslides shown occurred at high elevations ($>$1600 m) in areas with slopes ($>7\%$), and all appeared in the two land-use classes pasture or dry-farming agricultural lands. Accordingly, in the first stage of the rule-based landslide

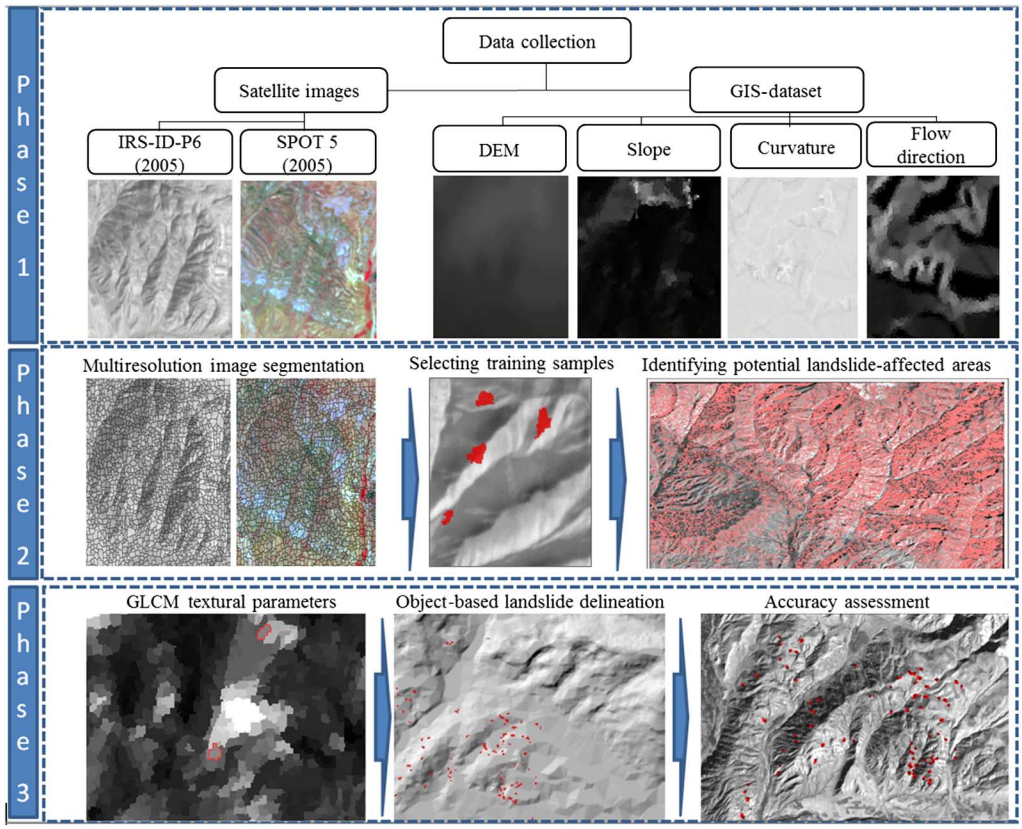

Fig. 1. Location of the Urmia Lake basin study area in north-western Iran (rectangle).

classification, areas above 1600 m and with a slope greater than 7% were therefore considered to be areas that might be affected by landslides, and only these "possibly affected by landslides" areas were considered further for the detection and delineation of landslides during the subsequent classification stages.

D. Rule-Based Classification of Satellite Imagery

1) Brightness-Based Classification: One important characteristic that can be commonly observed in postevent panchromatic images is an increase in the brightness of areas that have been affected by landslides, due to a loss of vegetation and exposure of fresh rock and soil [2], [29], [30]. This characteristic can be captured in an object-based environment through change analysis of pre- and postlandslide images, in order to detect where landslides have occurred [29]. As mentioned previously, most of the landslides in our study area can be classified as rotational slides. The contrast in vegetation between landslide-affected areas and their surroundings, together with light-toned scarps, is considered to be the diagnostic features of rotational slides [5]. The brightness parameter can therefore be used to detect landslides on the basis of these characteristics. Brightness for the IRS panchromatic image, and subsequently for the SPOT image, was calculated using the following equation [31]:

$$B = \frac{1}{n_{\text{vis}}} \sum_{i=1}^{n_{\text{vis}}} \bar{C}_{i(\text{vis})} \tag{1}$$

where B is the mean brightness of an object and $\bar{C}_{i(\text{vis})}$ is the sum of all the mean brightness in the visible bands divided by the corresponding number of bands n_{vis} [31]. The same spectral bands were then considered in calculating MaxDiff for each object, which is defined as the absolute difference between the minimum object mean ($\min(\bar{C}_{i(\text{vis})})$) and the maximum object mean ($\max(\bar{C}_{i(\text{vis})})$) divided by the mean object brightness B [31]

$$\text{MaxDiff} = \frac{|\min(\bar{C}_{i(\text{vis})}) - \max(\bar{C}_{i(\text{vis})})|}{B}. \tag{2}$$

In order to detect brightness anomalies, we used a function in the eCognition software developer environment called "brightness contrast to dark neighbors" in order to detect tonal variations between landslide-affected areas and adjacent areas [29]. The calculated brightness thresholds for landslide-affected objects indicated a value of 134 for the IRS-ID satellite image and 104 for the SPOT satellite image, respectively. Only objects with a brightness value above these thresholds were therefore considered as landslide candidate (LC) in the second step of the classification. Fig. 2 shows the satellite images and calculated brightness with two examples of landslide objects.

2) NDVI-Based Classification: The NDVI is commonly used to assist in landslide detection. Areas affected by natural landslides generally exhibit low NDVI values due to significant features that are observable on the ground following a landslide, such as areas devoid of vegetation and exposures of fresh rock or soil [29]. Vegetation differences between

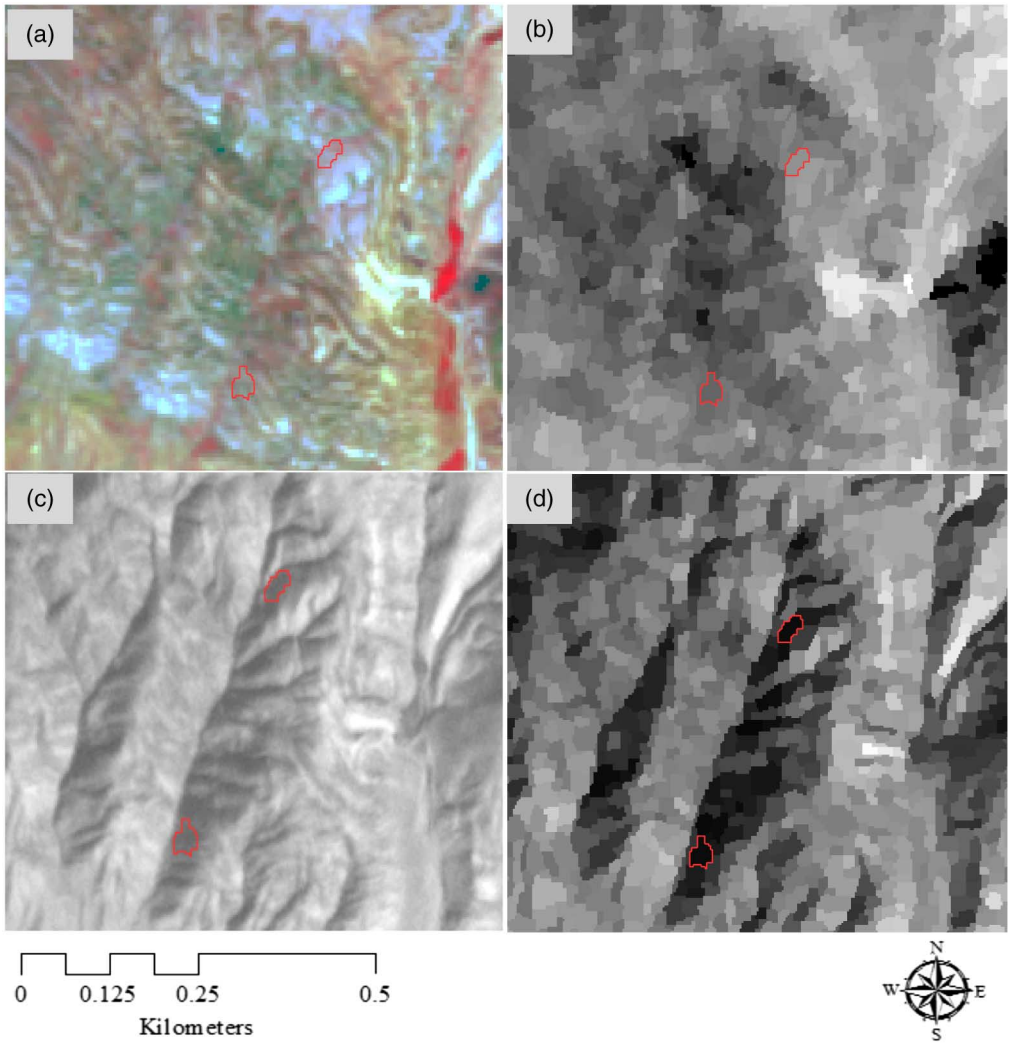

Fig. 2. Logical workflow and major steps of the analyses divided in three phases.

"possible landslide areas" and "nonlandslide areas" are clearly detectable on satellite images using the NDVI, which is able to reflect even minor changes in vegetation cover. This feature was therefore utilized to carry out a rule-based classification of the SPOT multispectral image. The NDVI was obtained using the infrared and red bands [see Fig. 3(a) and (b)]. The mean NDVI was selected as a threshold for the assumption that landslide objects appear darker than the background and have a lower NDVI than the mean NDVI. This iterative algorithm is a special one-dimensional case of the k-means clustering algorithm, which has been proved to converge to a local minimum. NDVI thresholding was performed using the following three steps [30]:

1) $$T_v = \text{mean NDVI} \tag{3}$$

2) $$f(\text{object}) = \begin{cases} \text{LC, if } f(\text{object}) \leq T_v) \\ \text{VA, if } f(\text{object}) > T_v) \end{cases} \tag{4}$$

3) $$T_v' = \frac{\text{mean NDVI}_{\text{LC}} + \text{mean NDVI}_{\text{VA}}}{2} \tag{5}$$

where T_v' is an average of the mean NDVI values for "LC" and vegetated areas (VA). The NDVI, which has a value between -1.0 and $+1.0$, was used to describe the vegetation density of the observed object. Since the mean NDVI value was used as a threshold in the classification of LC, i.e., areas with no significant vegetation cover, the identified target features exhibited low NDVI values similar to those for roads, river sand, built-up areas, and barren rocky lands, which were also detected. Accurate identification of false positives is therefore essential to reduce misidentification errors [29]. Objects with high NDVI values were considered to be spectral anomalies, and a threshold of mean NDVI > 0.05 was defined in order to exclude these anomalous false positives [see Fig. 3(b)]. We also used spatial properties such as compactness, the shape index, and roundness to characterize the morphometric properties of landslides in order to exclude nonlandslide objects.

E. Incorporating Textural Algorithms Into the Classification Process

A landslide changes the morphology of the affected area. The texture of a landslide-affected area on satellite imagery relates

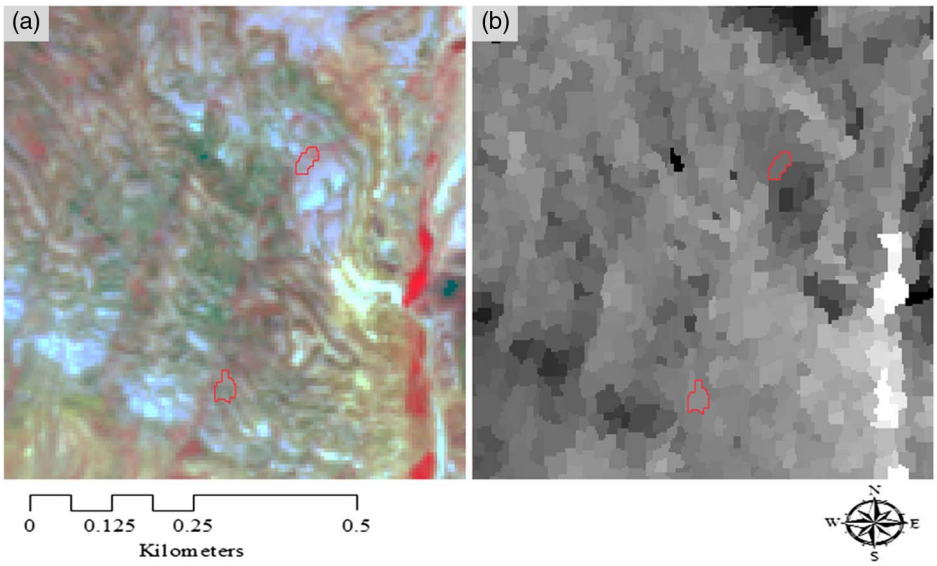

Fig. 3. Areas classified as "potentially affected by landslides" (highlighted in red) superimposed on the IRS panchromatic satellite image.

to the surface disturbance and the presence of cracks and/or ridges [32], with landslide-affected surfaces often showing textural patterns that are orientated down-slope. Such morphological features and their associated reflectivity patterns on satellite imagery are potential diagnostic features that could be used to distinguish them from surfaces with textural patterns that are oriented perpendicular to the slope direction [31]. Textural features were therefore selected to improve landslide classification and we used OBIA methodology to address such textural characteristics in a rule-based classification. One parameter that was found to be very useful was the "mean difference to neighboring objects," which revealed the degree of contrast between an object (such as a scarp or an accumulation zone) and its neighboring objects (such as the environment around the scarp or accumulation zone) [32].

In order to analyze textures we developed a rule-based classification using gray level cooccurrence matrices (GLCM). The use of GLCM can enhance the classification of single features on high resolution images [48]. A GLCM is a tabulation of how often different combinations of pixel brightness values (gray levels) occur within an image [33]. GLCMs are used to calculate the different directional components of the textural parameters [34]. A GLCM is a symmetrical $(\mathrm{n} \times \mathrm{n})$ matrix containing the relative frequencies of two pixels, linked by a spatial relationship within a local domain of the image, one of which has a gray level of i and the other a gray level of j, with $\mathrm{i}, \mathrm{j} \in \lfloor 0 \ldots \mathrm{n}-1 \rfloor$, where n is the gray-level number with which the image has been coded [34]. Several parameters can affect the textural measurements, including the window size, the statistical method used, the vector displacement, and the number of gray levels used to calculate the index. All of these parameters are related to the spatial and spectral resolution of the image, and to the spatial characteristics (e.g., dimensions, shape) of the different textures to be detected [34]–[36].

Stumpf and Kerle [31] have previously demonstrated the potential of directional flow-texture measurements to improve the assessment and quantification of landslide patterns. We have followed a similar approach to develop rule-based GLCM texture parameters based on flow directions (see Fig. 4). The combined directional texture parameter was derived from two different applications of directional GLCMs, one computed along the hydrological flow direction ($\mathrm{GLCM}_{\mathrm{flowdir}}$) and one perpendicular to it ($\mathrm{GLCM}_{\mathrm{flowdir}}$) [31], [33]. However, GLCM values do not make sense for nominal data. One solution is to use probabilities [33], which involves transforming the GLCM values into a close approximation to probabilities, a process known as normalizing the matrix. It is only an approximation because a true probability would require continuous values but the gray levels are integer values. This normalization can be calculated as follows [33]:

$$P_{i,j} = \frac{V_{i,j}}{\sum_{i,j=0}^{N-1} V_{i,j}} \tag{6}$$

where Pi, j is the probability value from the GLCM (i.e., how many times the reference value V occurs in a specific combination with a neighbor pixel), i is the row number, and j is the column number. The i and j numbers keep track of pixels by their horizontal and vertical coordinates. Since these numbers for the first cell in the upper left corner of the GLCM are (0, 0), the i value (0) of this cell is the same as the value of the reference pixel (0). Similarly, the second cell down from the top has an i value of 1 and a reference pixel value of 1. The range of summation $(\mathrm{i}, \mathrm{j} = 0 \text{ to } \mathrm{N}-1)$ means simply that each cell in the GLCM is considered; it is shorthand for a double summation: once from $\mathrm{i} = 0$ to $\mathrm{i} = \mathrm{N}-1$ and once from $\mathrm{j} = 0$ to $\mathrm{j} = \mathrm{N}-1$. A count would usually be expected to start with the number 1, with the summation running from 1 to N, but by designating the coordinates of the cell in the upper left corner of the matrix as $\mathrm{i} = 0$ and $\mathrm{j} = 0$ rather than $\mathrm{i} = 1$ and $\mathrm{j} = 1$, the i value remains the same as the actual gray level of the reference cell, and the j value remains the same as the gray level of the

neighbor cell. Following the normalization of the GLCM five textural parameters were identified that could be used to reveal any correlations between GLCMs and flow directions:

1) Contrast (Con): The contrast is also known as the "sum of squares variance" and can be calculated as follows:

$$\sum_{i.j=0}^{N-1} P_{i,j}(i-j)^2. \tag{7}$$

When i and j are equal, the cell lies on the diagonal of the matrix and $(\mathrm{i}-\mathrm{j})=0$. These values represent pixels that are entirely similar to their neighbors and hence they are ascribed a weighting of 0. Some other conditions also apply, such that if i and j differ by 1, there is little contrast and the weighting is 1. If i and j differ by 2, the contrast is higher and the weighting is 4. The weighting then continues to increase exponentially as $(\mathrm{i}-\mathrm{j})$ increases [33]. Results for the contrast $\mathrm{GLCM}_{\mathrm{flowdir}}$ are shown in Fig. 4(b).

2) Correlation (Cor): The correlation texture measures the linear dependency of gray levels on the gray levels of neighboring pixels and is calculated (following [33], [36]) as

$$\sum_{i.j=0}^{N-1} P_{i,j}\left[\frac{(i-\mu_i)(j-\mu_i)}{\sqrt{(\sigma_i^2)(\sigma_j^2)}}\right]. \tag{8}$$

When calculating the GLCM variance, $\mathrm{Pi,j}=0$ for each value except for the single entry of 1, μi, and μj are the means of row i and column j, and σi and σj are the standard deviations of row i and column j. The formula collapses to $=1(\mathrm{i}-\mu)2$, but since $\mu=\mathrm{i}$, this becomes 1 $(\mathrm{i}=\mathrm{i})2=0$. In a normalized GLCM, a uniform image area will have a single entry of 1 on the diagonal of the matrix, in a position corresponding to the row and column numbered with the original gray level (GL) value of the pixels in the image (e.g., if all GL values are equal to 2, then the number "1" will appear in position $\mathrm{i}=2$, $\mathrm{j}=2$ in the GLCM). The mean then becomes $\mu=\mathrm{i}=\mathrm{j}$ $(=2$ in the example given) [33]. Correlation results for $\mathrm{GLCM}_{\mathrm{flowdir}}$ are shown in Fig. 4(c).

3) Entropy (Ent): Entropy refers to the quantity of energy that is permanently lost to heat (or "chaos") every time a reaction or a physical transformation occurs. It is equal to [33] and [36]

$$\sum_{i,j=0}^{N-1} P_{i,j}(-1nP_{i,j}). \tag{9}$$

The term $\mathrm{P}*\ln(\mathrm{P})$ is maximized where its derivative with respect to P is 0. By the product rule, this derivative is $\mathrm{P}*\mathrm{d}(\ln(\mathrm{P}))/\mathrm{d}(\mathrm{P})+\mathrm{d}(\mathrm{P})/\mathrm{d}(\mathrm{P})*\ln(\mathrm{P})$, which simplifies to $1+\ln(\mathrm{P})=0$, yielding $\mathrm{P}=1/\mathrm{e}$. This means that the maximum of the term to be summed occurs when P is $1/\mathrm{e}$, which is about 0.378. However, the sum of $\mathrm{Pi,j}=1$, by definition. Under this constraint, the overall maximum of the sum (i.e. of Ent) is 0.5. This maximum is reached when all probabilities are equal [33]. Entropy values computed from $\mathrm{GLCM}_{\mathrm{flowdir}}$ are shown in Fig. 4(d).

4) Standard Deviation (StdDev): In order to calculate the standard deviation $\mathrm{GLCM}_{\mathrm{flowdir}}$, the GLCM variance was first calculated. The GLCM variance is equal to [36]

$$\sigma_i^2=\sum_{i,j=0}^{N-1} P_{i,j}(i-\mu_i)^2\sigma_j^2=(j-\mu_i)^2. \tag{10}$$

The standard deviation was then computed from these results using the following equations:

$$\sigma_i=\sqrt{\sigma_i^2} \tag{11}$$

$$\sigma_j=\sqrt{\sigma_j^2}. \tag{12}$$

The GLCM variance for textural measurements is based on the mean, and the dispersion around the mean, of cell values within the GLCM. The GLCM variance in textural measurements is based on the mean, and the dispersion around the mean, of cell values within the GLCM; it deals specifically with the dispersion around the mean of combinations of reference and neighbor pixels [33]. Fig. 4(e) depicts the standard deviation $\mathrm{GLCM}_{\mathrm{flowdir}}$ results calculated on the basis of the GLCM variance.

5) Mean: The GLCM mean was calculated as follows:

$$\mu_i=\sum_{i,j=0}^{N-1} i(Pi,j),\quad \mu_j=\sum_{i,j=0}^{N-1} j(Pi,j). \tag{13}$$

Equation (13) on the left calculates the mean based on the μ_{i} reference pixels, while the equation on the right uses the neighboring $\mu_{(\mathrm{j})}$ pixels. For the symmetrical GLCM, in which each pixel in the window is counted once as a reference and once as a neighbor, the two values are identical [34]. The mean $\mathrm{GLCM}_{\mathrm{flowdir}}$ results are shown in Fig. 4(f).

These GLCM parameters were computed in symmetric matrices for pixels that neighbored each other directly to the north, south east, and west, and to the NE, SE, SW, and NW. Based on the research by Stumpf and Kerle [31], the rotational invariance of a GLCM derivative can be determined by calculating its mean or minimum value in all four directional GLCMs ($\mathrm{GLCM}_{\mathrm{alldir}}$) prior to calculating the derivative. Five rotationally invariant textural parameters were thus calculated for landslide detection, based on the observation that landslide-affected zones typically show textural patterns with a down-slope alignment that are potential diagnostic features with which to distinguish such zones from unaffected land surfaces with textural patterns that are oriented parallel to the strike of the slope [32].

In order to utilize these patterns, further directional textural parameters were derived from two directional GLCMs, one computed along the hydrological flow direction ($\mathrm{GLCM}_{\mathrm{flowdir}}$) and the other perpendicular to it ($\mathrm{GLCM}_{\mathrm{flowdir}}$). The results of this stage were used to determine the correlation between the hydrological $\mathrm{GLCM}_{\mathrm{flowdir}}$, rotationally invariant and topographically controlled GLCM Cor derived in previous stages. GLCM parameters were subsequently calculated for each raster

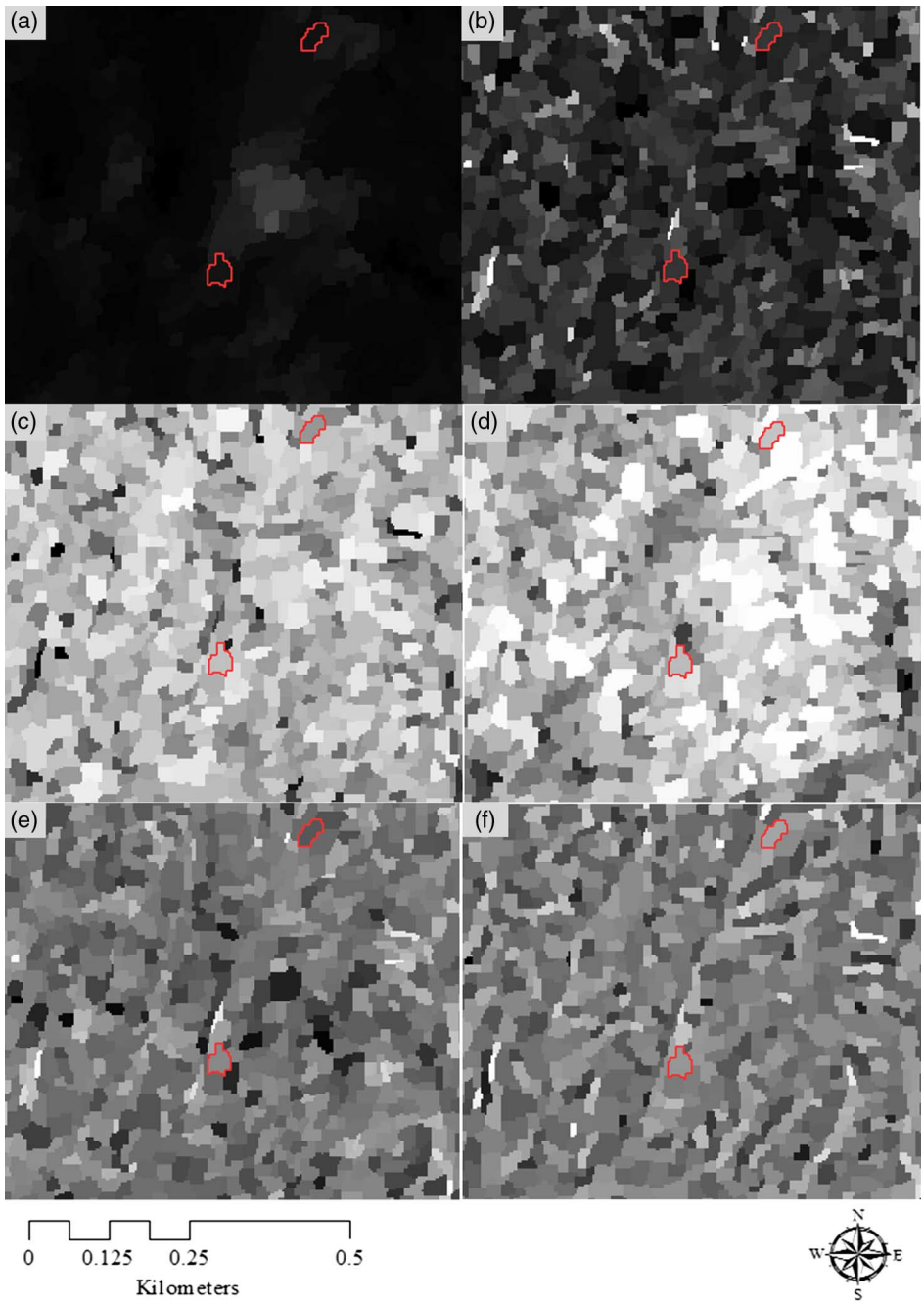

Fig. 4. Typical landslide complex within the study area [16].

cell, simply as the quotient of the texture parameters computed in flow direction and their counterparts computed in a direction perpendicular to the flow direction. The contrast, correlation, entropy, standard deviation, and mean values derived from $\mathrm{GLCM}_{\mathrm{flowdir}}$, together with their respective $\mathrm{GLCM}_{\mathrm{ratios}}$, are referred to as topographically guided texture parameters. These results were converted into raster layers and these layers, together with the texture parameters from $\mathrm{GLCM}_{\mathrm{alldir}}$, used to further refine the landslide detection. Finally, the identified landslide objects were refined using flow direction-based GLCM texture parameters. Fig. 5 shows the two landslide objects detected and their GLCM textural parameter values.

III. Results and Accuracy Assessment

Fig. 6 shows the results of the semiautomated object-based delineation of landslides for the study area. A total of 147 landslide objects were identified. The total area affected by these landslides was computed to be approximately 67.5 ha. The detected landslides vary in size between 310 and 5786 m^2.

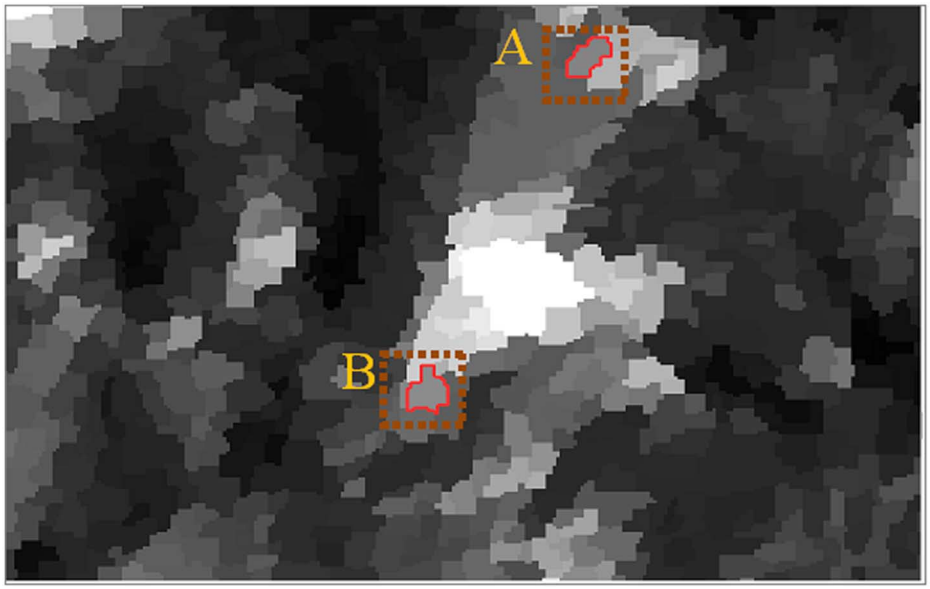

Objects	GLCM all dirc Con	GLCM all dirc Cor	GLCM all dirc Ent	GLCM all dirc StdDev	GLCM all dirc Mean
A	795.15	0.7466	5.492	29.97	129.52
B	799.98	0.8216	5.359	34.64	128.62

Fig. 5. (a) SPOT satellite image, (b) brightness calculated from SPOT image, (c) IRS-ID satellite image and (d) brightness calculated from the IRS-ID image (with maximum brightness shown as black and minimum brightness as white). Two examples of landslides are outlined in red.

When analyzing satellite images it is crucial that the accuracy of any classifications should be assessed [37]. Following Gao [38], we aimed to measure the quality of our methodology with respect to its suitability for the given application. The quality of landslide detection is evaluated on the basis of its spatial accuracy, and also on the type and accuracy of information shown on the resulting map [3], [39]. Defining the accuracy of a landslide inventory is not straightforward and no general standards exist [1], [3], [39]. For our study in northern Iran, we evaluated the accuracy of the OBIA-derived landslides by comparing them to an existing landslide inventory map of the study area as described in Section II-B. Although this inventory may not be exhaustive, it is considered to provide a good reference dataset for the situation that existed in 2005. The database consists of coordinates for representative points within known landslide areas. (As mentioned in Section II-B, it does not include the spatial footprints of the landslides and it was this absence that provided the motivation for this research.) The accuracy assessment could therefore only be conducted on the basis of a point-to-polygon comparison in GIS. Fig. 7 shows an area that has been affected by many landslides. This figure also shows a comparison between the detected landslides and the known landslide events (i.e., from the existing landslide inventory database). A total of 109 sets of GPS landslide coordinates were used as ground truth data with which to measure the accuracy of the semiautomatically detected landslides. The accuracy assessment reveals commission and omission errors, which are measurements of both the user's and the producer's accuracy [18]. The landslides delineated in our study yielded a user's accuracy of 92.8% and a producer's accuracy of 91.9%. By statistically summarizing the total number of landslides, user's and producer's accuracies of 93.01% and 92.8%, respectively, were achieved. The overall accuracy of the resulting map is 93.07% (see Fig. 7).

IV. Discussion

Since landslides are complex natural phenomena a range of parameters needs to be considered for their semiautomated detection. They represent complex geomorphologic processes, spectral characteristics from satellite images alone may not be sufficient for accurate identification of landslide locations [5]. Semiautomated object-based classification appears to be very suitable for this task. In order to maintain the transferability of this approach [39], [40], we used as few spectral parameters as possible (i.e., brightness and NDVI), complemented by spatial, morphometric, and textural parameters.

Three main stages were involved in the detection of landslides. In the first stage, slope and DEM parameters were used for rule-based classification of "possible landslides areas" and "nonlandslide areas." A total of 2662 image objects were identified as landslide candidates. In the second stage, spectral information including brightness and NDVI were used to classify the possible landslides. We then integrated textural parameters, based on the observations that landslides change the morphology of the affected areas and that landslide-affected surfaces often show downslope-aligned textural patterns.

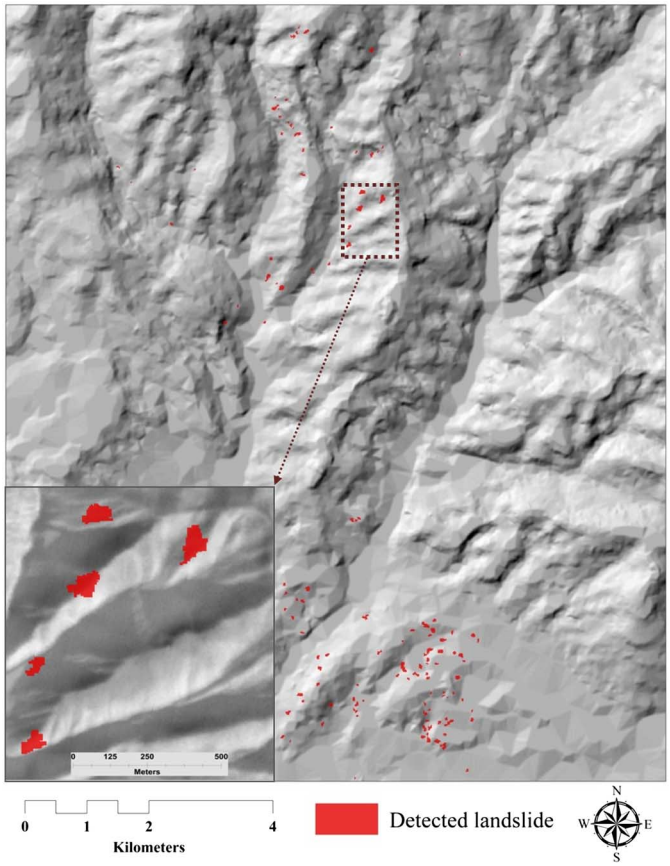

Fig. 6. (a) SPOT satellite image and (b) NDVI values derived from the SPOT image, averaged for each segmentation object. Bright areas indicate a high NDVI, darker areas indicate lower NDVI values.

NDVI values have previously been used by several researchers for semiautomated detection of landslides, in both pixel-based and object-based methods [2], [4], [5], [30]. Bare rock or debris are naturally exposed following a landslide (although at times mixed with remaining or dislodged vegetation), giving a bright appearance to landslide-affected areas on satellite imagery [2]. Fresh landslides can be well captured by remote sensing data, where the absence of vegetation cover can be used as a primary criterion for their recognition. The NDVI is useful for detecting land cover changes, and is even sensitive to small alterations in vegetation density [2].

In our study, the NDVI proved to be a very effective parameter for the detection of landslides, and in particular for recognizing landslide events within tuff formations characterized by low pasture vegetation cover. However, since NDVI uses only spectral information, objects with similar or even lower NDVI values (e.g., rocky outcrops, roads, water bodies, and river beds) are sometimes misclassified as landslides [2]. We found that the NDVI was very effective for recognizing landslide zones in tuff formations but tended to also include rock outcrops in the landslide classification. In order to reduce misclassifications, we incorporated additional rules, i.e., shape and textural parameters, which led to a clear improvement in accuracy. The integration of topographical GLCMs in particular, significantly reduced the misclassification of objects.

Methodologically, this study is one of the few to date that defines texture of individual objects—rather than being based on moving window kernels, as is common in the published literature [33]. The OBIA methodology and the programming environment (CNL in the eCognition software) allowed textural parameters to be computed for each object. These included GLCM homogeneity, GLCM dissimilarity, GLCM contrast, GLCM standard deviation, GLCM entropy, GLCM second angular momentum, GLCM correlation, and GLCM mean. GLCMs have only recently been adopted for landslide mapping [2], [5], [31], but our results have confirmed that (as pointed out by Stumpf and Kerle [31]), the use of GLCMs and their calculated derivatives offers a significant enhancement that makes the use of object metrics suitable for the incorporation of geomorphological phenomena. Topographically oriented GLCMs appear to be very efficient at landslide detection. In particular, the GLCM contrast between landslide areas and surrounding areas proved to be decisive. In addition, within the rule-based classification process the flow direction GLCM textural parameters were also useful to distinguish landslide areas. The optimal choice of the textural parameters depends on the application [31], and hence the method will remain only semiautomated.

Through the integration of these methods we have been able to achieve on overall accuracy of about 93%, obtained by comparing our results with the existing landslide inventory. However, it is important to point out that some information from the existing landslide inventory database was used to support the determination of a few of the thresholds (e.g., for slope, brightness) that were used during the semiautomated landslide detection. This had a minor positive influence on the accuracy values. The reliability of such inventory databases should be seen critical to their use as reference material as they are often outdated, inaccurate, or incomplete [4]). They are, however, often the only reference dataset available. Due to the lack of other reference data for the study area, we were only able to conduct a point-to-polygon comparison for assessing the accuracy of the detected landslides. To make more reliable statements about the quality of the landslide detection and delineation, more adequate reference data should be used in future; either collected through field investigations and GPS measurements or created by manual interpretation of landslides based on orthophotos. By integrating optical satellite imagery from different sensors with DEM data and its derivatives, we have been able to detect and to delineate landslides more efficiently than by relying on single data sources only. Nonetheless, some uncertainty may be introduced as a result of the DEM data representing a different point in time from the satellite imagery, and hence possibly excluding some recent landslides.

In summary, an OBIA methodology has been established based on the integration of remote sensing satellite imagery with GIS topographical datasets. The most suitable spectral, spatial, morphometric, and textural parameters gathered from different datasets were utilized in a rule-based classification, for semiautomated landslide identification and delineation. Due to the exposure of outcrop and fresh rock (although at times mixed with remaining or dislodged vegetation; [2]), landslide scarps and zones generally tend to have high brightness values

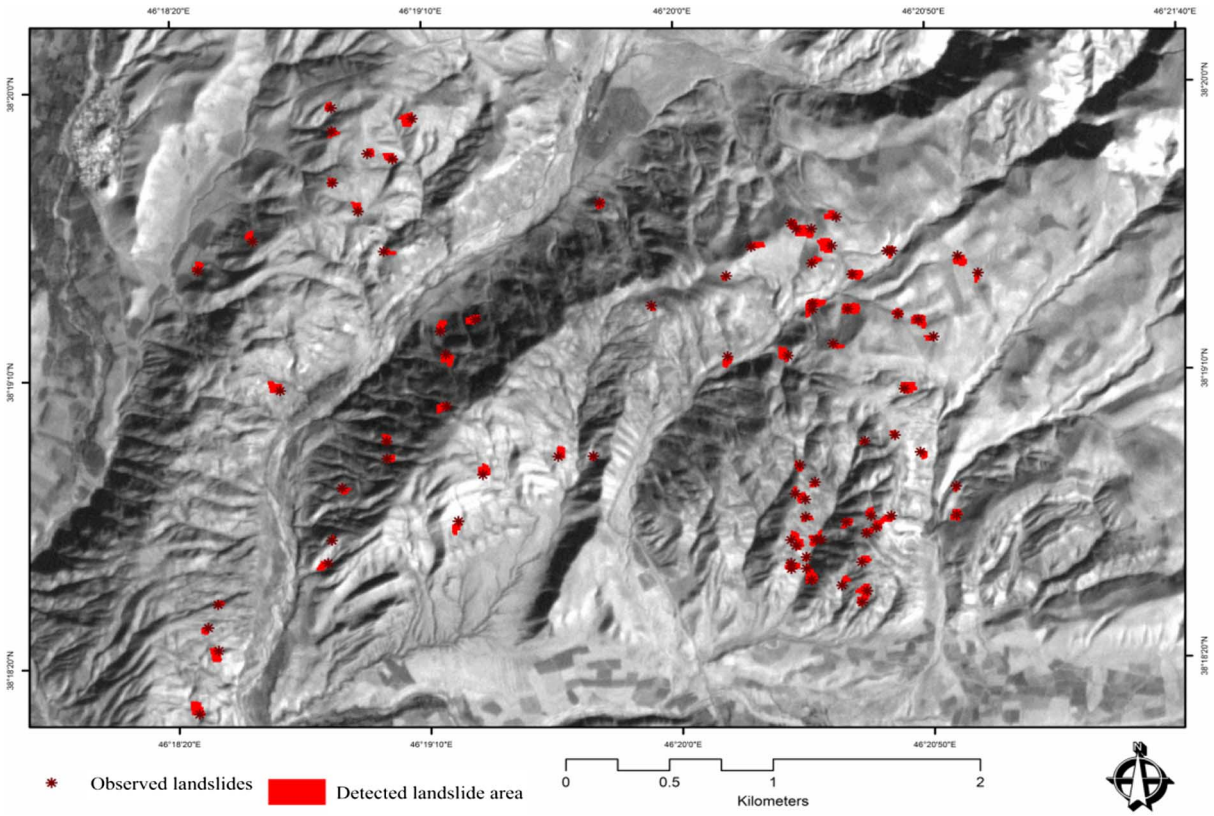

Fig. 7. Flow direction and its computed parameters: (a) flow direction, (b) contrast, (c) correlation, (d) entropy, (e) standard deviation, and (f) mean.

in satellite imagery, typically yielding higher reflectance values in the visible bands than surrounding areas with soil and vegetation cover [2], [41]. Roads or geological formations such as tuffs may also exhibit similar spectral reflectance characteristics to landslide areas, but the use of OBIA facilitates the discrimination and delineation of landslides by allowing additional parameters (other than spectral values) to be incorporated. Shape-based parameters such as shape index, roundness, and compactness were able to effectively characterize the morphometric properties of landslides. The particular novelty and flexibility of this method lies in its ability to combine the use of spectral information, shaped-based information, and topographically oriented GLCMs.

V. Conclusion

Landslides are destructive natural phenomena that frequently lead to serious problems in hilly areas, resulting in injuries or fatalities, economic losses, and high infrastructure maintenance costs, as well as causing severe damage to natural resources [2], [42]. The availability of new remote sensing technologies for the detection and mapping of landslides may facilitate the production of landslide maps, as well as the definition of suitable criteria for evaluating the quality of such maps [3]. OBIA offers comprehensive and flexible methods for landslide detection and mapping as it allows the integration of data from different sources, taking into account the most appropriate spectral, spatial, contextual, or textural properties while at the same time reducing the influence of single pixel reflectance. Within this study, a semiautomated object-based method was developed for the detection and delineation of landslides in northwestern Iran. Our results indicate that a combination of various parameters, and especially the integration of textural characteristics, leads to a high accuracy of landslide detection. The calculated overall accuracy amounted to approximately 93% which is very high. There is, however, potential to improve the accuracy either by considering additional parameters during the rule-based classification, or by using satellite images with a higher spatial resolution.

We consider GEOBIA to be a remarkable paradigm shift in remote sensing and geographic information science in recent years [6], [21], [22], [46]. We conclude that OBIA offers a unique opportunity to exploit spectral information from satellite imagery in combination with topographic information from DEMs and thus provides a suitable framework for landslide mapping. While the need for such integration has been previously recognized (see [42]–[46]), OBIA is today able to provide the necessary flexible computing environment. Our approach is semiautomated but incorporates a way of capturing complex information in a systematic and repeatable manner. In this respect, considerable progress has been made toward a spatially explicit information extraction workflow.

We conclude from this study that OBIA provides a particularly suitable framework for landslide mapping using a combination of remote sensing and GIS datasets. Information on spatial extent of landslides is known to be crucial for assessing landslide risk and for decision making that aims to reduce risk and mitigate further hazards. In this regard, a landslide

inventory map should record the locations, the dates (if known), and the types of all mass movements that have left discernible traces in an area [3]. In the absence of proper landslide inventories, OBIA can be used to detect and delineate landslides very efficiently. Since the landslide inventory database used for the study presented herein was limited to point-based GPS data recorded during field surveys, the delineation of landslide footprints was of great importance to (a) identify landslides that had not yet been documented, and (b) allow further information to be obtained on the delineated areas, e.g., through GIS-based overlays with other data sources.

REFERENCES

[1] M. Galli, F. Ardizzone, M. Cardinali, F. Guzzetti, and P. Reichenbach, "Comparing landslide inventory maps, *Geomorphology*, vol. 94, pp. 268–289, 2008.

[2] T. R. Martha, N. Kerle, J. Jetten, C. J. van Westen, and K. Vinod Kumar, "Characterising spectral, spatial and morphometric properties of landslides for semi-automatic detection using object-oriented methods," *Geomorphology*, vol. 116, pp. 24–36, 2010.

[3] F. Guzzetti *et al.*, "Landslide inventory maps: New tools for an old problem," *Earth Sci. Rev.*, vol. 112, no. 1, pp. 42–66, 2012.

[4] D. Hölbling *et al.*, "A semi-automated object-based approach for landslide detection validated by persistent scatterer interferometry measures and landslide inventories," *Remote Sens.*, vol. 4, pp. 1310–1336, 2012.

[5] B. Aksoy and M. Ercanoglu, "Landslide identification and classification by object-based image analysis and fuzzy logic: An example from the Azdavay region (Kastamonu, Turkey)," *Comput. Geosci.*, vol. 38, pp. 87–98, 2012.

[6] T. Blaschke, "Object based image analysis for remote sensing," *ISPRS J. Photogramm. Remote Sens.*, vol. 65, pp. 2–16, 2010.

[7] L. Draguţ and C. Eisank, "Automated object-based classification of topography from SRTM data," *Geomorphology*, vol. 141–142, pp. 21–33, 2012.

[8] J. Barlow, Y. Martin, and S. E. Franklin, "Detecting translational landslide scars using segmentation of Landsat ETM+ and DEM data in the northern Cascade Mountains, British Columbia," *Can. J. Remote Sens.*, vol. 29, no. 4, pp. 510–517, 2003.

[9] J. Barlow, S. Franklin, and Y. Martin, "High spatial resolution satellite imagery, DEM derivatives, and image segmentation for the detection of mass wasting processes," *Photogramm. Eng. Remote Sens.*, vol. 72, pp. 687–692, 2006.

[10] S. Lang, "Object-based image analysis for remote sensing applications: Modeling reality—Dealing with complexity," in *Object-Based Image Analysis—Spatial Concepts for Knowledge-Driven Remote Sensing Applications*, T. Blaschke, S. Lang, and G. J. Hay, Eds. Berlin, Germany: Springer-Verlag, 2008, pp. 3–28.

[11] A. S. Laliberte *et al.*, "Object-oriented image analysis for mapping shrub encroachment from 1937 to 2003 in southern New Mexico," *Remote Sens. Environ.*, vol. 93, pp. 198–210, 2004.

[12] P. Lu, A. Stumpf, N. Kerle, and N. Casagli, "Object-oriented change detection for landslide rapid mapping," *IEEE Geosci. Remote Sens. Lett.*, vol. 8, no. 4, pp. 701–705, Jul. 2011.

[13] G. J. McDermid and S. E. Franklin, "Spectral, spatial, and geomorphometric variables for the remote sensing of slope processes," *Remote Sens. Environ.*, vol. 49, pp. 57–71, 1994.

[14] I. V. Florinsky, "Combined analysis of digital terrain models and remote sensing data in landscape investigations," *Prog. Phys. Geogr.*, vol. 22, pp. 33–60, 1998.

[15] B. Feizizadeh and T. Blaschke, "Landslide risk assessment based on GIS multi-criteria evaluation: A case study in Bostan-Abad County, Iran," *J. Earth Sci. Eng.*, vol. 1, no. 1, pp. 66–71, 2011.

[16] B. Feizizadeh and T. Blaschke, "GIS-multicriteria decision analysis for landslide susceptibility mapping: Comparing three methods for the Urmia lake basin, Iran," *Nat. Hazards*, vol. 65, no. 3, pp. 2105–2128, 2012.

[17] B. Feizizadeh, T. Blaschke, and H. Nazmfar, "GIS-based ordered weighted averaging and Dempster Shafer methods for landslide susceptibility mapping in Urmia lake Basin, Iran," *Int. J. Digit. Earth*, vol. 7, no. 8, pp. 688–708, 2014.

[18] Ministry of Natural Resources (MNR), East Azerbaijan Province. Landslide event report of East Azerbaijan Province, Tabriz, Iran, 2010.

[19] U. C. Benz, P. Hofmann, G. Willhauck, I. Lingenfelder, and M. Heynen, "Multi-resolution, object-oriented fuzzy analysis of remote sensing data for GIS-ready information," *ISPRS J. Photogramm. Remote Sens.*, vol. 58, no. 3/4, pp. 239–258, 2004.

[20] Y. Liu, Q. Guo, and M. Kelly, "A framework of region-based spatial relations for non-overlapping features and its application in object based image analysis," *ISPRS J. Photogramm. Remote Sens.*, vol. 63, no. 4, pp. 461–475, 2008.

[21] G. J. Hay and T. Blaschke, "Foreword special issue: Geographic object-based image analysis (GEOBIA)," *Photogramm. Eng. Remote Sens.*, vol. 76, no. 2, pp. 121–122, 2010.

[22] M. Baatz and A. Schäpe, "Multiresolution segmentation: An optimization approach for high quality multi-scale image segmentation," in *Proc. 12th Symp. Appl. Geogr. Inf. Process. [Angew. Geogr. Inf. (AGIT)]*, Salzburg, Austria, 2000, pp. 12–23.

[23] D. Arvor, L. Durieux, S. Andrés, and M. A. Laporte, "Advances in geographic object-based image analysis with ontologies: A review of main contributions and limitations from a remote sensing perspective," *ISPRS J. Photogramm. Remote Sens.*, vol. 82, pp. 125–137, 2013.

[24] Definiens, *Developer 7. Reference Book*. München, Germany: Definiens Imaging GmbH, 2007.

[25] L. Drăguţ, T. Schauppenlehner, A. Muhar, J. Strobl, and T. Blaschke, "Optimization of scale and parametrization for terrain segmentation: An application to soil-landscape modelling," *Comput. Geosci.*, vol. 35, no. 9, pp. 1875–1883, 2009.

[26] L. Dragut, D. Tiede, and S. R. Levick, "ESP: A tool to estimate scale parameter for multiresolution segmentation of remotely sensed data," *Int. J. Geogr. Inf. Sci.*, vol. 24, pp. 859–871, 2010.

[27] R. Soeters and C. J. van Westen, "Slope instability recognition, analysis and zonation," in *Landslides, Investigation and Mitigation*, A. K. Turner and R. L. Schuster, Eds. Washington, DC, USA: National Academy Press, 1996, pp. 129–177.

[28] M. Akbarimehr, M. Motagh, and M. Haghshenas-Haghighi, "Slope stability assessment of the Sarcheshmeh landslide, Northeast Iran, investigated using InSAR and GPS observations," *Remote Sens.*, vol. 5, pp. 3681–3700, 2013.

[29] T. R. Martha, K. Kerle, C. J. van Westen, V. Jetten, and K. V. Kumar, "Object-oriented analysis of multi-temporal panchromatic images for creation of historical landslide inventories," *ISPRS J. Photogramm. Remote Sens.*, vol. 67, pp. 105–119, 2012.

[30] T. R. Martha and N. Kerle, "Segment optimisation for object-based landslide detection. In: GEOBIA 2010: geographic object - based image analysis," in *Proc. Int. Arch. Photogramm. Remote Sens. (ISPRS)*, E. A. Addink and F. M. B. Van Coillie, Eds., 2010, vol. XXXVIII-4/C7, 6pp.

[31] A. Stumpf and N. Kerle, "Object-oriented mapping of landslides using random forests," *Remote Sens. Environ.*, vol. 115, pp. 2564–2577, 2011.

[32] M. Moine, A. Puissant, and J. P. Malet, "Detection of landslides from aerial and satellite images with a semi-automatic method. Application to the Barcelonnette basin (Alpes-de-Haute-Provence, France)," in *Landslide Processes: From Geomorphological Mapping to Dynamic Modelling*, J. P. Malet, A. Remaitre, and T. Bogaard, Eds. Strasbourg, France: CERG, 2009, pp. 63–68.

[33] M. Hall-Beyer. (2010, May 15). *GLCM Tutorial 2007* [Online]. Available: http://www.fp.ucalgary.ca/mhallbey/tutorial.htm

[34] M. Pesaresi, A. Gerhardinger, and F. Kayitakire, "A robust built-up area presence index by anisotropic rotation-invariant textural measure," *IEEE J. Sel. Topics Appl. Earth Observ. Remote Sens.*, vol. 1, no. 3, pp. 180–192, Sep. 2008.

[35] D. Chen, D. A. Stow, and P. Gong, "Examining the effect of spatial resolution and texture window size on classification accuracy: An urban environment case," *Int. J. Remote Sens.*, vol. 25, no. 11, pp. 2177–21, 2004.

[36] M. Pesaresi, "Textural classification of very high-resolution satellite imagery. Empirical estimation of the interaction between window size and detection accuracy in urban environment," in *Proc. Int. Conf. Image Process.*, Kobe, Japan, Oct. 1999, vol. 1, pp. 114–118.

[37] T. M. Lillesand and R. W. Kiefer, *Remote Sensing and Image Interpretation*, 4th ed. Hoboken, NJ, USA: Wiley, 2001.

[38] Y. Gao, "Pixel based and object oriented image analysis for coal fire research," M.S. thesis, ITC, Enschede, Netherlands, 2003.

[39] J. Walker and T. Blaschke, "Object-based landcover classification for the Phoenix metropolitan area: Optimization vs. transportability," *Int. J. Remote Sens.*, vol. 29, no. 7, pp. 2021–2040, 2008.

[40] P. Hofmann, T. Blaschke, and J. Strobl, "Quantifying the robustness of fuzzy rule sets in object based image analysis," *Int. J. Remote Sens.*, vol. 32, no. 22, pp. 7359–7381, 2011.

[41] D. Tiede, S. Lang, and C. Hoffmann, "Type-specific class modelling for one-level representation of single trees," in *Object-Based Image Analysis: Spatial Concepts for Knowledge-Driven Remote Sensing Applications*, T. Blaschke, S. Lang, and G. J. Hay, Eds. Berlin, Germany: Springer-Verlag, 2008, pp. 133–151.
[42] G. Chen, G. J. Hay, L. M. Carvalho, and M. A. Wulder, "Object-based change detection," *Int. J. Remote Sens.*, vol. 33, no. 14, pp. 4434–4457, 2012.
[43] S. Lang and T. Blaschke, "Bridging remote sensing and GIS—What are the main supporting pillars?" *Int. Arch. Photogramm. Remote Sens. Spat. Inf. Sci.*, vol. XXXVI-4/C42, 2006.
[44] R. F. Chen *et al.*, "Topographical changes revealed by high-resolution airborne LiDAR data: The 1999 Tsaoling landslide induced by the Chi-Chi earthquake," *Eng. Geol.*, vol. 88, pp. 160–172, 2006.
[45] S. Lang, F. Albrecht, S. Kienberger, and D. Tiede, "Object validity for operational tasks in a policy context," *J. Spat. Sci.*, vol. 55, pp. 9–22, 2010.
[46] T. Blaschke *et al.*, "Geographic object-based image analysis: A new paradigm in remote sensing and geographic information science," *ISPRS Int. J. Photogramm. Remote Sens.*, vol. 87, no. 1, pp. 180–191, 2014.
[47] T. R. Martha, N. Kerle, C. J. van Westen, V. Jetten, and K. V. Kumar, "Segment optimization and data-driven thresholding for knowledge-based landslide detection by object-based image analysis," *IEEE Trans. Geosci. Remote Sens.*, vol. 49, no. 12, pp. 4928–4943, Dec. 2011.

Thomas Blaschke received the Ph.D. degree in geoinformatics in 1995.

He is a Professor with the University of Salzburg and the Deputy Director of the Interfaculty Department of Geoinformatics—Z_GIS, and the Head of the Research Studio iSPACE. Prior positions include Lecturer, Senior Lecturer, and Professor positions in Germany, Austria, and the U.K., as well as temporary affiliations as Guest Professor and Visiting Scientist. He is the author, coauthor, or editor of 17 books and 75 journal publications. His research interests include the integration of GIS and remote sensing.

Mr. Blaschke has received several academic awards e.g., the Christian-Doppler Prize 1995.

Bakhtiar Feizizadeh received the Ph.D. degree in applied geoinformatics from the University of Salzburg, Salzburg, Austria, in 2014.

He is currently an Assistant Professor with the Department of remote Sensing and GIS, University of Tabriz, Tabriz, Iran. He has published more than 50 scientific publications in the domain of geoinformatics. His research interests include methodological issues in geoinformatics, integration of GIS and remote sensing for land use/cover monitoring, land suitability analysis, geohazard and risk assessment, and, in particular, landslide mapping.

Daniel Hölbling received the M.Sc. degree in applied geoinformatics from the University of Salzburg, Salzburg, Austria, in 2006.

He is currently a Researcher with the Interfaculty Department of Geoinformatics—Z_GIS, University of Salzburg, Salzburg, Austria. Being involved in several national and EU-funded research projects related to the European Earth Observation Programme Copernicus, he is active in the fields of natural hazards and risks, environmental applications, and human security. He specializes in remote sensing and object-based image analysis. His research interests focus on EO-based monitoring of natural disasters, landslides and land use/land cover analysis.